JOURNAL OF MATERIALS SCIENCE 16 (1981) 589–598

The properties of stainless steel compacted dynamically to produce cold interparticle welding

D. RAYBOULD
Institut CERAC, Chemin des Larges Pièces, 1024 Ecublens, Switzerland

The impact of a high-speed punch on metal powder has been shown to result, under optimized conditions, in interparticle melting and welding. A strong compact is thus obtained which requires no subsequent thermal treatment. The technique can produce parts from non-equilibrium powders or powder mixtures. However, even with standard powder, such as stainless steel, the technique imparts unique properties to the resultant part. For instance, the macrohardness (420 HV) indicates an exceptionally high degree of work-hardening and that the interparticle melted zones are rapidly quenched. Annealing the compacts for 1 hour at temperatures up to 900° C does not result in a significant change in the yield stress.

1. Introduction

Conventional powder metal processes all consist of variations of the two basic operations of compaction and sintering. Recently, however, it has been shown [1, 2] that the impact of a high-speed punch on powder can, during room temperature compaction, produce interparticle melting and bonding of a similar type to that which occurs during friction and explosive welding. This allows the high-temperature sintering operations and related high-temperature operations such as sinter forging to be completely avoided. Thus alloys or powder mixtures can be produced which would degenerate or react chemically if produced by conventional techniques where they would be exposed to high temperatures. Therefore, the dynamic compaction technique extends the range of special alloys that can be produced by powder metallurgy. For example, steel powder (or even iron oxide) may be add-mixed with aluminium powder to produce an aluminium alloy which has good wear and seizure resistance (conventional sintering of such a material would result in a thermite-type reaction [2]). Similarly, diamonds may be placed in steel without the formation of cast iron. Additionally, rapidly quenched or amorphous powders may be consolidated without degeneration or crystallization of their microstructure [2].

The technique not only allows the consolidation of non-equilibirum materials, but also imparts some special characteristic [1, 2]. In particular, the high strain rates and absence of a subsequent annealing operation result in a material of high strength and hardness. In addition, the particles are cold-welded together and, at high rates of compaction, a characteristic layer of material is formed between the particles which have melted during compaction and subsequently solidified.

To determine the characteristics of the compaction technique itself, a series of experiments on standard powders was carried out. Stainless steel, type 304L, was found to be a typical material in its response to dynamic compaction as well as having well-documented properties for conventionally produced powder metal parts and wrought material.

2. Theoretical considerations

In 1729 the Rev. J. T. Desaguliers [3] recognized the if two freshly cut metal surfaces are placed in intimate contact, then a force of several pounds is required to separate them. However, in order to produce effective bonds, melting or near-melting

0022–2461/81/030589–10$03.00/0

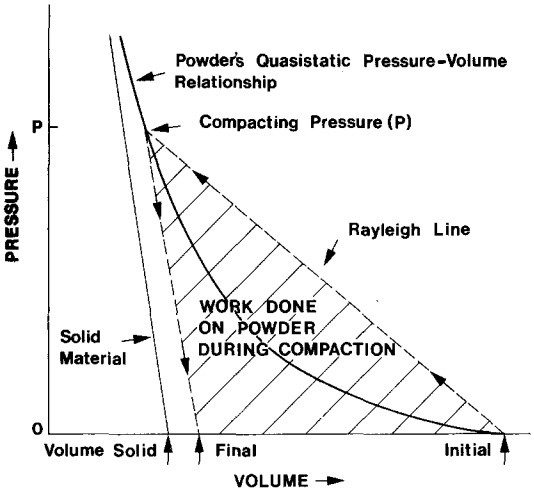

Figure 1 Schematic pressure–volume relationship, showing the loading (Rayleigh line) and unloading paths.

conditions are normally required at the interface, even if this is only for a very short time, as during the seizure of bearings.

For powder compaction, the overall temperature rise is small, even during high-speed compaction where adiabatic conditions exist [4]. However, if it is assumed that most of the work of compaction occurs at the circumference of the particle by interparticle friction and local deformation of asperities, then it should be possible, by increasing the rate of compaction still further, to avoid heat conduction to the centre of the particle and thus produce melting at the particle's circumference. The overall work of compaction may be calculated from the area under the Rayleigh line of the pressure–volume (displacement) curve (Fig. 1). This Rayleigh line may be assumed to be the straight line joining the two points on the pressure–density curve.) If this work is all deposited at the interface then the maximum time of compaction may be calculated for which heat conduction to the centre of the particle is so small that the interface is at or above the melting temperature [5]. This time is of the order of microseconds or less, thus implying that the conditions of interparticle melting may only be obtained by a discrete, well-defined shock wave. An obvious way of obtaining such a shock wave is by a high-velocity impactor striking the powder [5].

The compactions were carried out by a machine driven by compressed air. This consisted of a driver unit and a guide tube down which a plastic punch travelled to impact on the powder placed in a 50 mm diameter compaction chamber. Both

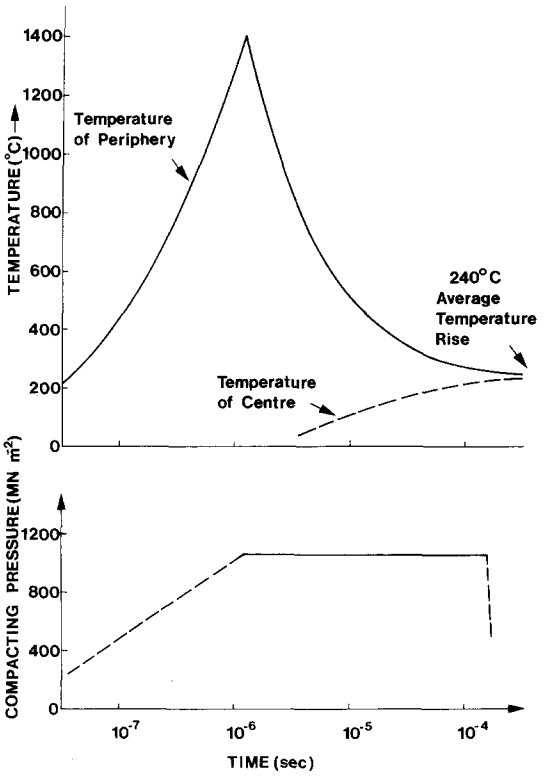

Figure 2 The predicted temperature and pressure histories, during compaction, for the periphery and centre of a 100 μm stainless steel particle.

single- and double-stage driver units were used [4, 6]. For this work, compaction was effected by the passage of one shock wave through the powder. The conditions of compaction were chosen so that interparticle melting occurred and a high-density part (over 97.5% theoretical density, TD) was produced [1, 5]. The compaction pressure for the majority of the compacts in this investigation was 1200 $MN m^{-2}$, which, for a shock wave following the Rayleigh line [4] (Fig. 1), produces a calculated average temperature rise of 250° C [5]. For interparticle melting to occur under these conditions the work of compaction must be carried out in less than one microsecond [5].

Typical average temperature and pressure histories of the surface of a spherical stainless steel particle are shown in Fig. 2 [5]. It can be seen that the pressure and temperature both pass through the powder as shock waves with similar rise times and that when the maximum pressure has been obtained, no more work is done and the temperature of the circumference rapidly falls. Conduction results in the temperature at the

centre of the particle increasing after the circumference has passed its maximum temperature. So the temperature at the centre of the particle follows behind and has a longer rise time than the pressure wave.

The duration of the pressure pulse depends upon the time taken for the arrival of the relief wave from the rear of the impactor. This time is determined by the length and material of the impactor [4]. In Fig. 2 a typical value for this work has been shown.

Fig. 2 particularly illustrates the high rate of deformation, over $10^6\,sec^{-1}$, and the short duration of the pressure, 10^{-4} sec. It also shows the rapid rate of quenching to which the interparticle melting zone is subjected. For the case in question, this is $2 \times 10^8\,^\circ C\,sec^{-1}$ down to 700° C and $2 \times 10^7\,^\circ C\,sec^{-1}$ down to the less significant value of 300° C. The average temperature rise of 240° C is maintained until significant conduction occurs to the compaction chamber.

It can thus be seen from Fig. 2 that the technique can produce very high rates of work-hardening, that the pressure duration is very short (so that the compaction chamber and support may be smaller than is normally necessary for the pressure contained) and that the high temperatures are present for extremely short times, thus allowing the consolidation of non-equilibrium alloys.

3. Experimental details

The 304L stainless steel powder used was commercially available, atomized, 100 μm powder. However, other powders and particle sizes were also investigated. No lubricants were add-mixed with the powder, but die lubrication was employed. Compaction was effected, as outlined above, using a compressed-air-driven machine of the type shown in Fig. 3, which impacted a high velocity punch onto the powder [4].

The properties of the as-compacted material were obtained by standard testing techniques. The compacts produced at the conditions required to produce interparticle melting could be sawn, turned or milled into test specimens by normal workshop techniques.

4. Properties

4.1. Final density

It has previously been shown [4, 7] that the high-speed compaction of powders can result in a higher density for a given compaction pressure

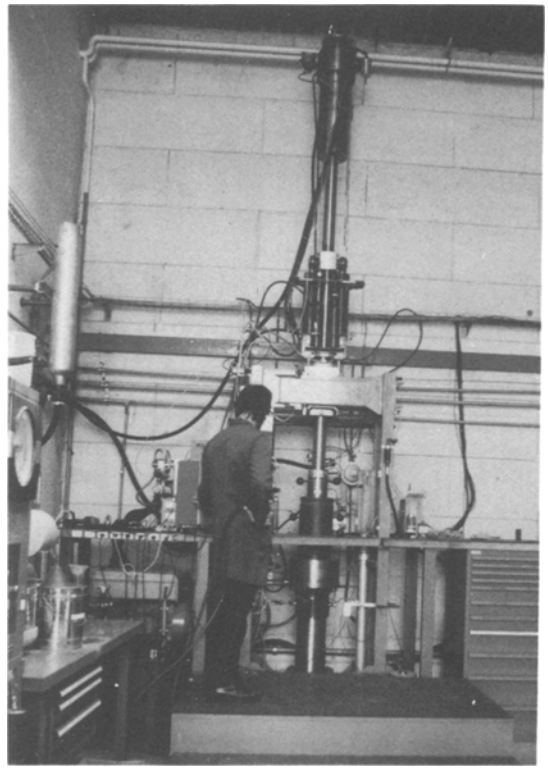

Figure 3 A dynamic compaction press of over 1000 ton capacity.

than is possible by quasi-static compaction, this being especially so at densities over 90% TD. The reported increases have been 2 or 3%, but smaller increases have been obtained for stainless steel dynamically compacted under conditions that do not result in interparticle melting [8]. However, when interparticle melting occurs the resultant density increase is much greater, of the order of 5 to 7% (Fig. 4). It can be seen that this halves the pressure required to obtain high densities.

It may be assumed that the molten metal acts as an interparticle lubricant, or perhaps that the high temperature at the circumference decreases the flow stress of the material. In any case, it appears that as the interparticle melting increases, the pressure required to obtain a given density decreases.

4.2. Tensile strength

The green strength of the compact is dependent upon the effectiveness of the interparticle welds and this is related to the rate of compaction, which is determined by the rise time of the compacting shock wave [1]. However, metallurgically, the strain rate is usually used to describe the

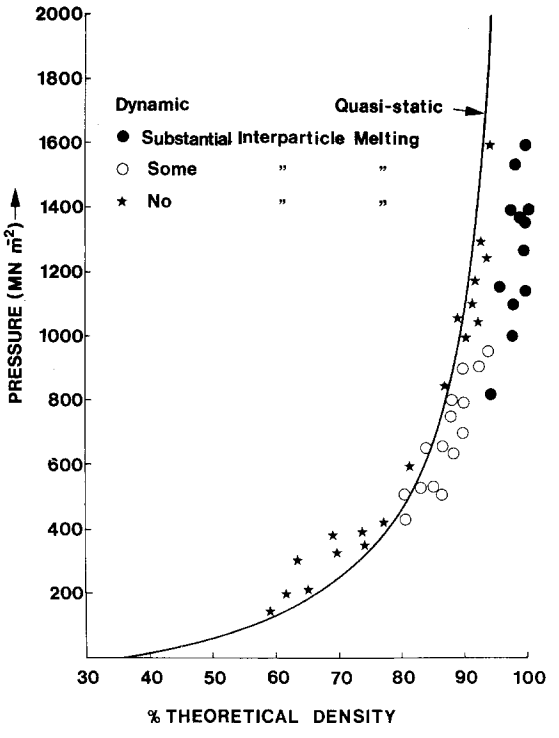

Figure 4 The pressure–density relationship for stainless steel showing the density increase that occurs with increasing amounts of interparticle melting.

effect of changes in the rate of deformation. The average strain during compaction may be obtained from the initial and final densities. The time of deformation may be obtained from the time taken by a compacting shock wave to pass a characteristic dimension of the powder, such as the particle size [5]. The velocity of the shock wave passing this point may be obtained from the pressure–density relationship of the powder and the compacting pressure [4].

The tensile tests were conducted on specimens machined from the compact into standard tensile specimens (Fig. 5). The strength can be seen (Fig. 6) to start to increase at average strain rates over $10^6\,\text{sec}^{-1}$ and to approach that of the wrought solid at strain rates of $10^8\,\text{sec}^{-1}$. It is to be expected that it will continue to increase as the strain rate increases. Interparticle melting was predicted to occur at strain rates over $10^6\,\text{sec}^{-1}$ [1, 5].

The ductility of the high-strength compacts was around 1 to 2% which, although low, is probably acceptable and, if necessary, could be improved by increasing the strain rate further or by partially annealing the compacts.

4.3. Fracture toughness

The plane strain fracture toughness K_{1c} of several compacts was determined by a bend test, according to ASTM standard E 399-74. The requirements of this test were met by the specimens. The fracture toughness appears to be directly related to the tensile strength. Therefore it can be expected to change with the rate of compaction in the same manner as the tensile strength (Fig. 6).

The lower-strength compacts (tensile strength equal to $320\,\text{MN m}^{-2}$) have a fracture toughness of $22\,\text{MN m}^{-3/2}$, which compares to sintered powder metal material with a theoretical density of 95% TD [9]. Higher-strength compacts (tensile strength equal to $500\,\text{MN m}^{-2}$) have a fracture toughness of $31\,\text{MN m}^{-3/2}$, comparable to that of the wrought material ($32\,\text{MN m}^{-3/2}$) [9]. Compacts with strengths above these values (600 MN

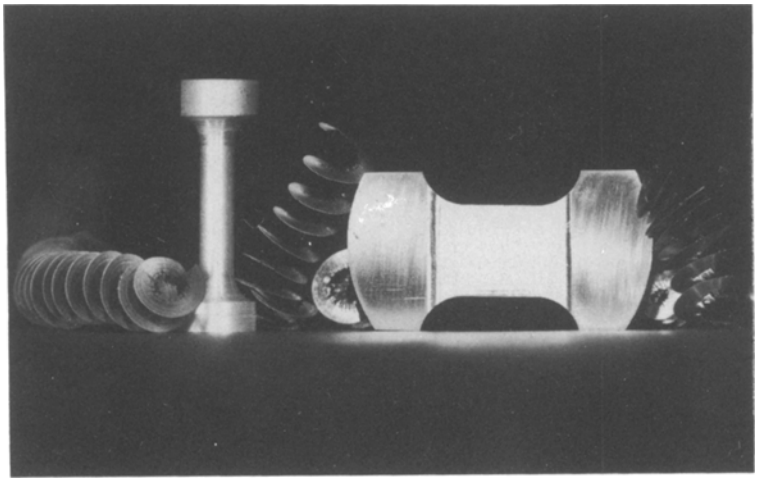

Figure 5 Tensile specimens machined from the as-compacted material. The specimens are 50 mm long. Note the continuous machining chips obtained.

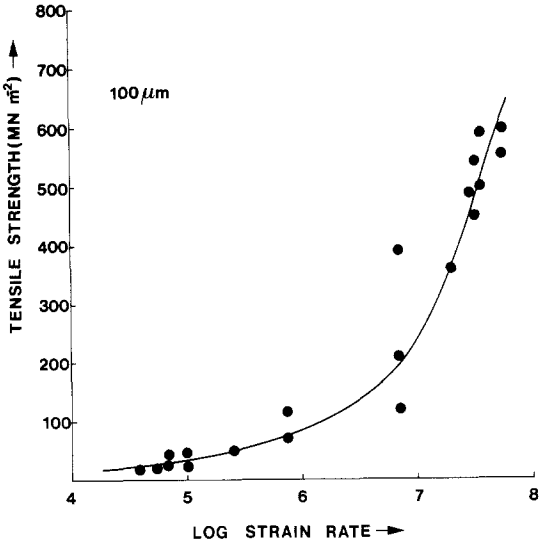

Figure 6 The as-compacted tensile strength as a function of the overall strain rate during compaction. All the compacts have a density of > 99% TD.

m^{-2}) were unfortunately not tested, but it can be expected that these would be equivalent or superior to the wrought material. Thus, while the compacts have a low ductility, their toughness appears acceptable.

4.4. Hardness

It is well-known that the passage of a shock wave can work (shock) harden metal. In fact, this has been used commercially for some time; small explosive charges are used to shock-harden the teeth of earth-moving equipment and the points of railway lines, etc. Explosive powder compacting also produces shock-hardening, although there is little detailed work on the comparison of the hardness of explosive and quasi-static compacts of the same density. Presumably, the poor tensile strength of the explosive compacts results in difficulties in obtaining as-compacted hardness values, while after sintering, the hardness approaches that of the quasi-static compact. However, Witkowsky and Otto [10] have found that iron powder has a hardness of 105 HV after explosive compaction, but after sintering at 1120° C this drops to 65 HV. This was for a 95% TD compact which they compared to an 85% TD conventional compact. The latter had an as-compacted hardness of 65 HV, which fell to 40 HV after sintering. Several workers [11, 12] have commented on the X-ray line broadening resulting from the increased stored energy (lattice defects) of explosive contacts.

TABLE I Comparison of the hardness of the dynamic compacts with the solid.

Type of material	Macrohardness (HV)
Dynamic compact	420
50% cold-worked solid	345
Explosive-hardened solid	350
Annealed solid	150

The dynamic compacts produced by the impact of a punch probably undergo even higher strain rates than compacts produced using explosives. Also, the resultant work-hardened structure is retained as no high-temperature operations are required to obtain an acceptable tensile strength. The stainless steel compacts had an average macrohardness of 420 HV. The microhardness is even higher, with an average of five compacts giving a value of 530 HV (0.05 g)*. These are to be compared with a macrohardness of 150 HV for a conventionally sintered compact of the same density, and to a similar value (130–170 HV) for the annealed solid. The dynamic compact, therefore, has a macrohardness nearly three times that of the annealed material. In comparison, shock-hardened solid stainless steel, subject to impact by a flyer plate to give a pressure of 45 000 MN m^{-2} for 10 μsec, experiences a macrohardness increase from 170 to 350 HV [13]. Similarly, cold-rolled 18/8 stainless experiences a macrohardness increase

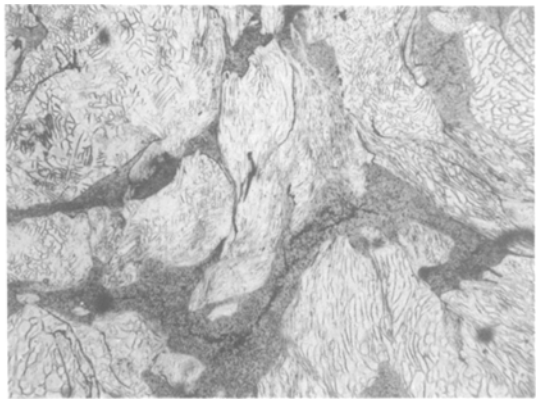

Figure 7 Optical micrograph (× 250) showing typical interparticle melting. The structure of the melted/weld zones is not resolvable.

*Figures in parentheses represent the load applied.

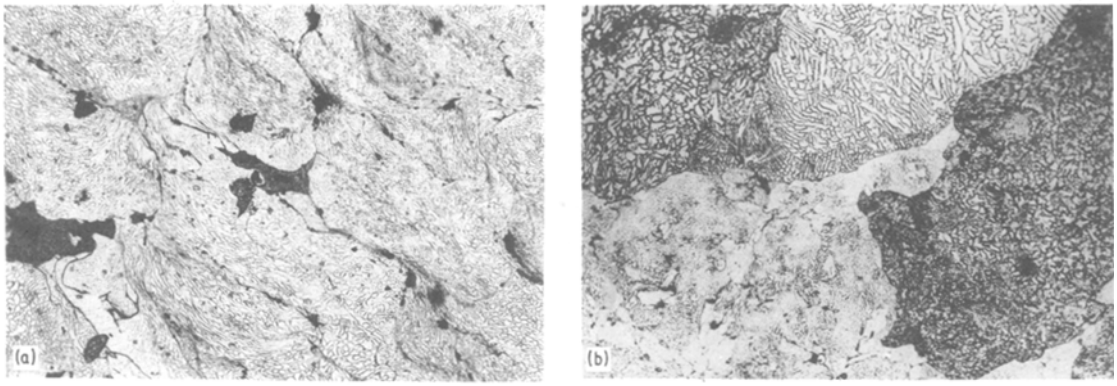

Figure 8 For certain strong compacts no melted zones are detectable. (a) Some melting (× 210). (b) Two different types of stainless steel powder mixed together (× 170).

from 170 HV to 285 HV for a 25% reduction and to 345 HV for a 50% reduction. The high hardness (Table I) of the compacts can probably be explained merely in terms of the very high strain rates (10^7 sec^{-1}). However, one may also consider the greater shear that can occur with powders as compared to solids. This indicates that a higher hardness should be obtained for a shock-deformed powder than for a solid.

In view of the increase of the strength with strain rate, a similar dependency could be expected for the hardness. Initially, the macrohardness is dependent upon the strength, but once the strength has reached a value of around 200 MN m^{-2} the hardness becomes independent of the strength and strain rate within experimental error. Presumably, the strength is dependent upon the interparticle welds while the hardness depends more upon the work-hardening which the particles undergo. However, it is surprising that an increase in the strain rate by a factor of ten (Fig. 6) does not change the degree of work-hardening as measured by the macrohardness. A possible explanation is that for this deformation mode, the material's maximum hardness has been approached and further increases in the rate of work-hardening result in a corresponding recovery, either static or dynamic. Alternatively, it could be that increases in the strain rate result in the formation of more material which has been molten during compaction and that it is the hardness of this material which has solidified after compaction which is starting to determine the hardness of the compact. Further evidence is presented below which shows that the re-solidified material is softer than the deformed but unmelted particles.

4.5. Microstructure

The microstructure of the compacts is typified by the interparticle melted zone just as explosive welds are characterized by their waves. Material which has melted during compaction and then solidified can be seen in Fig. 7 as a thin strip running between the particles. In certain cases, however, (Fig. 8) no such strip is visible and there is no evidence of interparticle melting. Provided the compaction has been carried out correctly, these bonds appear to be as strong as those when melting is observed. The fractured surface of such a compact where very little evidence of melting was found was studied by scanning electron microscopy. Ductile fracture regions were found, indicat-

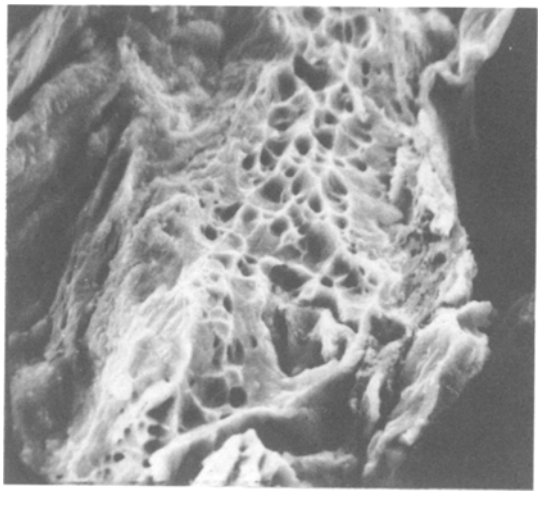

Figure 9 Scanning micrograph (× 3600) showing typical ductile fracture region associated with the melted zone. For this particular micrograph no melted zones were detected in the compact by optical microscopy (Fig. 7).

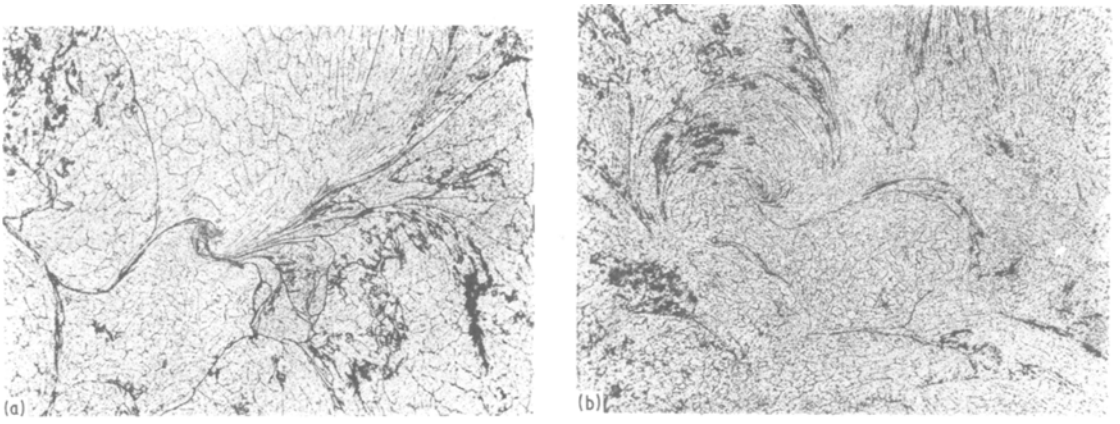

Figure 10 Two examples of extensive material flow at the interparticle boundaries resulting in waves, reminiscent of explosive welds (× 190).

ing that strong ductile bonds existed (Fig. 9). Such ductile fracture regions, often situated at the interparticle boundaries, are typical of the dynamic compacts. In certain cases, when no melted or weld zone is detectable, evidence can be found of extensive shear and, in some cases, interlocking waves of a similar type to those observed in explosive welding (Fig. 10). However, when melting is observed the compacts are usually stronger than when no melted zones are present. In contrast, explosive welding tries to avoid melting at the weld as this reduces the weld's strength.

The structure of the melted material is usually not detectable by optical microscopy and, as the cooling rate is of the order of $10^{8}\,^{\circ}\mathrm{C\,sec^{-1}}$ (Fig. 2), a very fine, $< 1\,\mu m$, or amorphous structure is to be expected. In only a very few cases was the grain structure of the melted zone detectable optically (Fig. 11). The structure can be seen to be a typical "as-cast" structure with solidification starting at the particle's surface and finishing in the centre at the original interparticle boundary. Here, very small microporosities have been detected and sometimes the oxide from the original surface of the particle remains.

Those melted zones which have a detectable structure are usually the larger melted regions where the cooling rate will be somewhat lower; they are often connected to thinner, molten regions which have no optically visible microstructure. Similarly, in Fig. 12, it can be seen that the microstructure is detectable only at the centre of the molten zone, thus indicating lower cooling rates or high impurity levels, as would be expected in an as-cast structure.

To try to determine the properties of the melted or weld zone, microhardness measurements were made of typical melted regions and of the particles (Fig. 13). Indents not completely within the melted zone were ignored. Loads of 100 and 200 g were used, and, especially for the melted zone, there was no significant difference between these. The average of these two loads and of several compacts gives the hardness of the particle as 420(40)* HV (0.15 g)* and of the melted zone as 340(10) HV (0.15 g). The hardness of the particles is the same as that reported in Section 4.4 for a 2 kg load. The melted material has a significantly lower hardness, but this is much higher than that of the as-cast or annealed values of 150 HV. As the material solidified after the compaction was

Figure 11 A rare example (× 300) where columnar-like, "as-cast" grains were detected in the melted zone.

*The figures in parentheses represent the standard deviation and load applied, respectively.

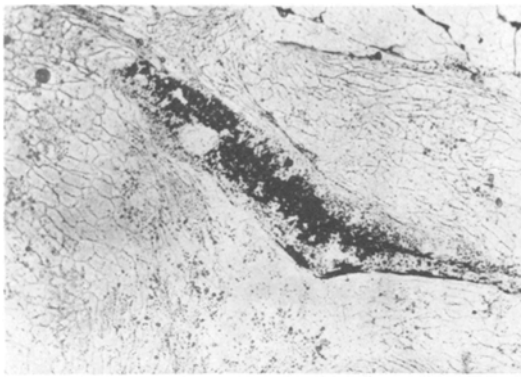

Figure 12 A rare case where grains were detected at the centre of the melted zone (× 300).

completed and there is no metallurgical evidence of work-hardening of the melted (weld) zone, it may be assumed that the relatively high hardness of this zone is due to its rapid quenching (Fig. 2). In the few cases where some structure was detectable in the melted zone, for instance as in Fig. 12, the larger grains at the centre of the zone had a size of the order of 3 μm.

Hall–Petch relationships for stainless steel are dependent on the chemical compositions and structure within the grains [14]. Extrapolation of these relationships to 3 μm gives values of 380 and 210 HV, respectively. A similar Hall–Petch relationship based on the powder particle size [8] gives, on extrapolation to 3 μm, a value of 380 HV. The hardness of the melted zone was of necessity measured in relatively large melted zones (Fig. 14). The minimum size of such a zone was of the order of 30 μm. Substituting this in the extrapolated Hall–Petch relationships gives 190 HV and 90 HV for the explosively hardened and annealed cases and 130 HV for the extrapolated particle size. The

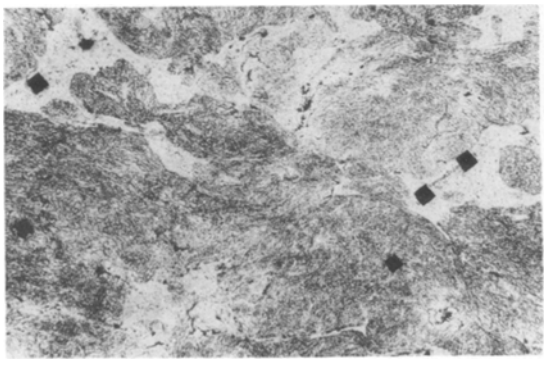

Figure 13 Optical micrograph (× 130) showing microhardness indents within the melted zone and particles.

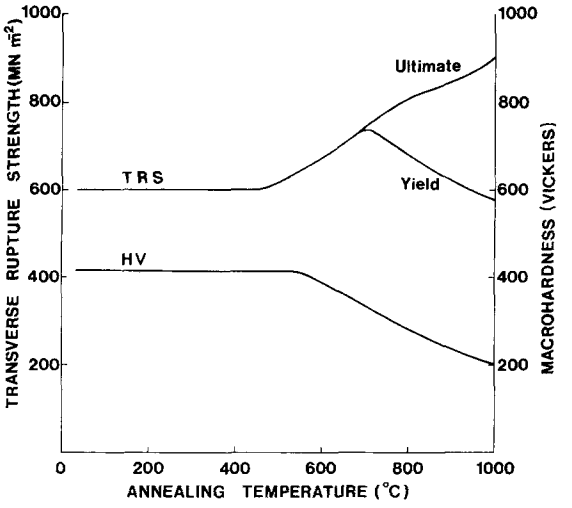

Figure 14 The transverse rupture stress and hardness as a function of annealing temperature.

hardness of the melted zone from which the grain size was obtained was around 370 HV(0.15) [the size of this melted zone was 30 μm (Fig. 12)]. In general, the hardness of melted zones where grains were detectable was higher than those where grains were not detectable. For some such zones, values of 500(50) HV (0.15 g) were obtained and in this case the grain size was estimated as being at most 1 μm × 10 μm. However, the scarcity of melted zones containing resolvable grains did not allow these values to be confirmed.

The extrapolated Hall–Petch relationships can

TABLE II Comparison of the hardness of the melted zone with that predicted by extrapolated Hall–Petch relationships.

	Region	Hardness (HV 0.15)
Observed values	Melted zone, usual structure	340(10)*
	Melted zone, grains detectable	500(50)
	Melted zone, mixed structure	370(20)
Extrapolated Hall–Petch values	Typical observed grain size (3 μm) from explosive-hardened equation	380
	Typical observed grain size (3 μm) from annealed equation	210
	Minimum size of melted zone for HV measurement (30 μm) from explosive-hardened equation	190
	Minimum size of melted zone for HV measurement (30 μm) from annealed equation	90

*Figures in brackets indicate standard deviation.

TABLE III The annealed hardness of dynamic and quasi-static compacts after sintering at 1100° C for 1 hour. Note: the microhardness values indicate the particle hardness and ignore the effect of porosity.

Hardness (load)	Dynamic, with interparticle melting (98% TD, annealed 1100° C)	Dynamic, no interparticle melting (92.5% TD, sintered 1100° C)	Quasi-static (92.5% TD, sintered 1100° C)
HV(2 kg)	180	155	95
HV(0.05 kg)	250	280	170
HV(0.025 kg)	330	290	200

only be expected to give an order of magnitude value. However, they do indicate (Table II) that the melted zone must be made up of a fine-grained or amorphous structure rather than one large grain. In addition, the higher hardness of the melted zone where a structure is visible is not inconsistent with the normal melted zone which has no detectable structure, being amorphous [15].

For stainless steel, therefore, the rate of work-hardening results in particles having a higher hardness than the rapidly quenched, melted (weld) zone. However, this will not necessarily be the case with other metals. For example, with lead the particles and melted zones both have the same microhardness of 27 HV. In the case of heat-treatable alloys it is conceivable that an extremely hard and brittle melted zone could be formed, although, at present, no such zone has been observed.

4.6. Annealing

It is because the compacts do not require sintering or subjection to high temperatures during fabrication that their response to annealing becomes of interest. Test specimens were cut from the same compact and annealed for 1 hour at a variety of temperatures. A protective atmosphere of 10% hydrogen in nitrogen was used in the furnace and the specimens were cooled in air. Fig. 14 shows typical dependences on annealing temperature for hardness, yield stress and ultimate stress in three-point bending. The hardness begins to decrease above 600° C, and at 700° C the yield stress decreases in a similar manner. The corresponding increase in ductility is shown by the increase in the ultimate stress. It is of interest to note that between 500 and 700° C the yield stress actually increases. Partly because of this, the yield stress after annealing at 900° C is the same as that of the as-compacted material.

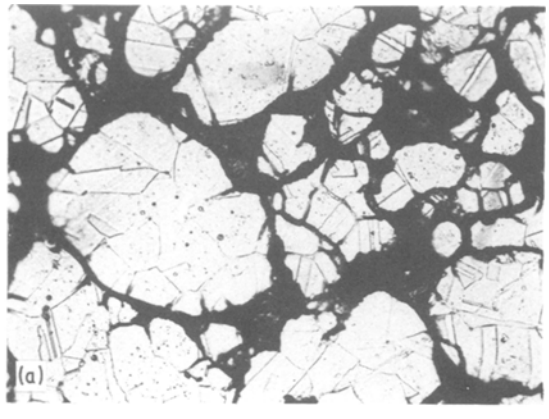

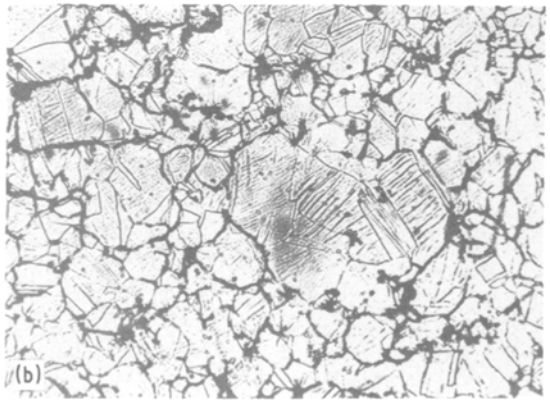

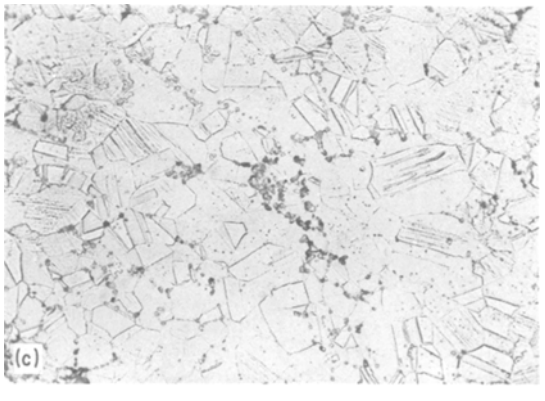

Figure 15 Optical micrographs (all × 320) showing annealing twins in (a) a 92.5% TD quasi-static compact, (b) a 92.5% TD dynamic compact where no interparticle melting occurred and (c) within a 98% TD dynamic compact which underwent interparticle melting. All the micrographs are taken on the compact's surface and illustrate the lower surface density of the quasi-static compact due to die friction.

The actual values of the yield and ultimate stress, even after a high-temperature anneal are found to be very dependent on the as-compacted strength and powder type. The hardness, however, appears to be primarily dependent on the annealing temperature. Even after annealing, the hardness of the compacts tends to be higher than that of the fully annealed solid or sintered part. This is detectable for dynamically compacted material which has not undergone interparticle melting. The macro- and microharness of such a dynamic compact are compared in Table III with a quasi-static compact of the same density (92.5% TD) sintered at the same temperature of 1100° C. Values are also given for a high-density dynamic compact which has undergone interparticle melting and has been annealed at 1100° C. The higher hardness, especially microhardness, of the annealed dynamic compacts is due presumably to a greater number and more even distribution of annealing twins, as shown in Fig. 15, where micrographs of the quasi-static and dynamic compacts are compared.

5. Conclusions

Compaction by a discrete shock wave results first in cold-bonding and then, at higher rates of compaction, in interparticle melting and a fusion-type weld. The resultant compacts not only have a high strength but have unique properties, even when conventional powders are compacted. In addition, it has been shown that:

(a) The effectiveness of the interparticle welds and hence the strength of the compacts increases with the rate of compaction.

(b) The molten material acts as an interparticle lubricant and can significantly increase the density at a given pressure.

(c) The powder particles are extremely work-hardened and for 304L stainless steel have a macrohardness above that obtained by shock-hardening or cold-rolling.

(d) The melted zones are rapidly quenched and have a high hardness, although for 304L stainless steel this is lower than that of the work-hardened particles. Fracture micrographs show that these zones are ductile. They could be responsible for the compacts having some ductility despite the extreme work-hardening of the particles.

(e) The yield stress does not significantly change after annealing for 1 hour at temperatures up to 900° C. However, above 600 to 700° C, the hardness decreases while the ductility increases.

(f) The fracture toughness is comparable to that of the wrought material.

References

1. D. RAYBOULD, 7th International Conference of the International Association for the Advancement of High Pressure Science and Technology, High Pressure Conference, Le Creusot, France, July, 1979 (Pergamon Press, Oxford, 1979).
2. D. RAYBOULD, D. MORRIS and G. A. COOPER, *J. Mater. Sci.* **14** (1979) 2523.
3. Rev. J. T. DESAGULIERS, *Proc. Roy. Soc.* (1724).
4. D. RAYBOULD, Proceedings of the 15th Machine Tool Design and Research (MTDR) Conference, Birmingham, September, 1975, edited by S. A. Tobias and F. Koenigsberger (Macmillan, London, 1975).
5. German Patent No. P.27 37674.9.
6. A. E. SEIGEL, Agardograph 91, Nato-Agard Fluid Dynamics Panel, Nato (1965).
7. S. ELSAKIL and R. DAVIES, Proceedings of the 13th MTDR Conference, (Macmillan, London, 1972).
8. D. RAYBOULD, Proceeding of 17th MTDR Conference, (Macmillan, London, 1977).
9. G. A. CLARKE and R. A. QUEENY, *Int. J. Powder Metall.*, **8** (1972) 81.
10. D. S. WITKOWSKY and H. OTTO, 4th High-Energy Rate Forming Conference, Denver Research Institute, Denver 1973.
11. P. A. VITYAZ and O. V. ROMAN, Proceedings of 13th MTDR Conference, (Macmillan, London, 1972).
12. R. A. PRUEMMER and G. ZIEGLER, *Powder Metall. Int.* **1** (1977) 11.
13. C. H. MA and L. E. MURR, 5th HERF Conference, Denver Research Institute, Denver 1975.
14. H. J. KESTENBACH and M. A. MEYERS, *Metall. Trans.* **7A** (1976) 1943.
15. R. L. FREED and J. B. VANDER SANDE, *Acta Metallogr.* **28** (1980) 103.

Received 19 June and accepted 18 July 1980.